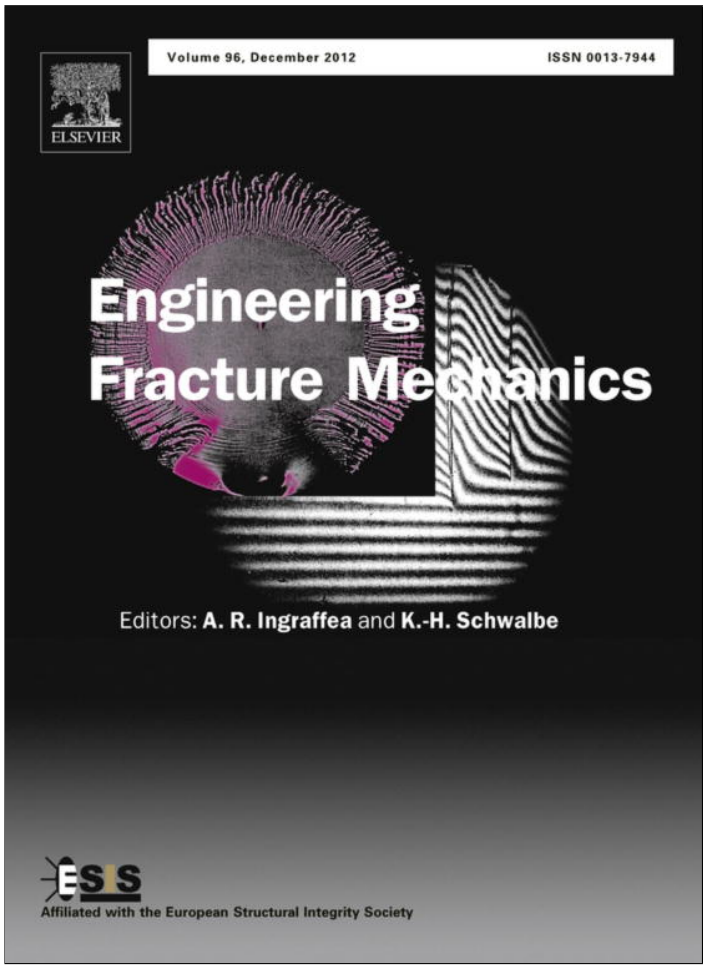

Engineering Fracture Mechanics 96 (2012) 490–499

Contents lists available at SciVerse ScienceDirect

Engineering Fracture Mechanics

journal homepage: www.elsevier.com/locate/engfracmech

Modeling crack propagation for advanced 4-point bending testing of metal–dielectric thin film stacks

K.R. Gadelrab [a,*], M. Chiesa [a], M. Hecker [b], H.-J. Engelmann [b]

[a] Laboratory for Energy and Nano Science (LENS), Masdar Institute, Abu Dhabi 54224, United Arab Emirates
[b] Center for Complex Analysis, GLOBALFOUNDRIES Dresden Module One LLC & Co. KG, Wilschdorfer Landstr. 101, D-01109 Dresden, Germany

ARTICLE INFO

Article history:
Received 26 December 2011
Received in revised form 11 August 2012
Accepted 16 August 2012

Keywords:
4-Point bending
Adhesion
On-chip interconnects
Finite-element modeling

ABSTRACT

For monitoring and improving mechanical properties of BEoL (back-end of line) interconnect structures in microprocessor technology, it is crucial to analyze their adhesion and crack propagation properties. In the present investigation, a camera assisted 4-point bending beam technique has been used to obtain fast and reliable adhesion measurements including locally resolved crack length information. To interpret the obtained crack propagation data, a finite-element modeling approach has been utilized. The combination of local measurement of the crack energy release rate and modeling enables to evaluate measurement curves for both symmetric and asymmetric crack propagation modes and to describe the crack propagation properties of the involved film stacks not attainable in such detail by conventional 4-point bending technique.

1. Introduction

The 4-point bending (4pb) delamination test is widely utilized for studying the interface properties of thin film structures such as semiconductor devices [1,2]. The importance of adhesion analysis as by 4pb has gained weight since the introduction of new materials in the field of semiconductors such as *low-k* and *ultralow-k* dielectrics [1], having a low mechanical stiffness and intrinsically poor adhesion to other materials [3,4]. This test has also been used to study the time dependent debonding of thin film interconnect structures [5] and the dependence of crack velocity on the film thickness [6,7].

A force curve extracted from a 4pb test can provide vital information on the mechanical properties of the test sample; however, the critical strain energy release rate G_c is particularly important to characterize the interface quality of the film stack [5]. Charalambides et al. [8] have provided a closed form solution to G_c as a function of the material properties, sample geometry and the applied load for 4pb conditions, resulting in the case of a sample of a single material and equal thicknesses of the two beams in:

$$G_c = \frac{21P_c^2L^2}{16Eb^2h^3} \tag{1}$$

where P_c denotes the critical load, L the distance between the inner and outer pins, E the effective Young's modulus, b the sample width and h the single beam height (cf. Fig. 1).

For the derivation of Eq. (1), it is assumed that, two cracks are propagating symmetrically along the beam axis within materials or interfaces of G_c values equal for both cracks. These assumptions are too ideal for day to day experiments and in reality are difficult to achieve. Misalignment and shape distortions can result in asymmetric crack growth, at least for stiff

* Corresponding author. Tel.: +971 561073723; fax: +971 26988121.
E-mail address: kgadelrab@masdar.ac.ae (K.R. Gadelrab).

0013-7944/$ - see front matter © 2012 Elsevier Ltd. All rights reserved.
http://dx.doi.org/10.1016/j.engfracmech.2012.08.018

Nomenclature

b	sample width
c	pre-crack length
g	measured gap in 4-point bending
h	single beam height
l	cantilever length
y	pin displacement
I	moment of inertia
E	effective Young's modulus
L	distance between the inner and outer pins
M	bending moment on a deflected cantilever
G_{I}	energy release rate for mode I
G_{II}	energy release rate for mode II
G_c	critical strain energy release rate
L_i	inner pins separation
P_c	critical load
τ	maximum traction in cohesive zone model
φ	phase angle in mixed mode fracture
δ	cantilever deflection
CZM	cohesive zone modeling
FEM	finite element modeling
BEoL	back-end of line
4pb	4-point bending

specimens [9]. Imperfections in the initiation of the crack and variation of material properties can also result in asymmetric pre-crack growth or crack propagation at different interfaces. It is of interest to utilize a modeling approach to investigate such non-ideal situations and assess the errors that might result in the measured G_c.

Finite element modeling FEM has been utilized to address crack propagation and interface delamination in semiconductor devices [2–4,10,11]. Particularly cohesive zone modeling CZM has proven to be an added value in modeling fractures in different material behaviors [4,12–17]. A CZM describes a gradual degradation in the adhesion between two surfaces along their interface. A traction separation law describes the relation between the bonded surfaces separation and the traction vector acting on them [4]. Therefore, the CZM can be utilized to describe the 4pb experiment especially when the crack propagation path is predefined.

In the present work, we utilize FEM to simulate a conventional 4pb test assuming idealized conditions. After numerical verification, we address the case of asymmetric pre-crack as a common situation in real experiments. Furthermore, we study the case where the crack propagates in one direction only or at two different interfaces. Comparison with data obtained from an advanced 4pb technique including crack length measurements enables to verify the FEM approach and to obtain explanations for experimental observations in the crack propagation plots. We demonstrate that Eq. (1) is applicable to much wider situations. Besides, crack length measurements are an added value to give indications of deviations in the test case.

2. Materials and method

A beam bending test setup has been utilized including measurement of the actual beam displacement, the loading force, and the length of both cracks propagating within the layer stack of a 4pb adhesion test. The crack length measurement was

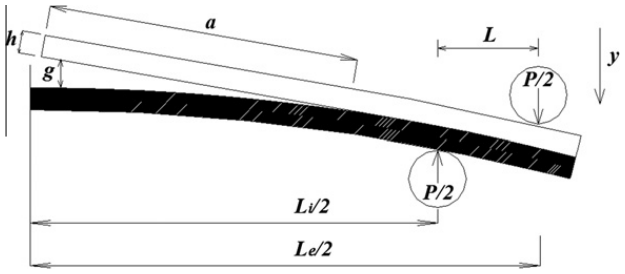

Fig. 1. A schematic representing an idealized 4pb test with the geometric parameters and with the symmetry applied on the left hand side. The gap opening and the crack length are denoted by g and a, respectively.

obtained utilizing a telecentric objective and a camera set-up enabling direct measurement of the actual gap g (cf. Fig. 1) with a rate of 5 measurement points/s. Data evaluation is attained using LabVIEW© where G calculation according to Eq. (1) is simultaneously performed along with the crack length measurements.

The films measured consist of *low-k* dielectric film, deposited on top of a Cu/dielectric film stack onto Si-001 substrates. The test is performed at a speed of 0.25 μm/s. Details for the 4pb experiments are given in [18].

3. Finite element modeling approach

A 4pb test of a bilayer Si strip is simulated using a commercial FE code, Ansys. The geometric model consists of two rectangles of 775 μm thickness each, representing a Si beam (cf. Fig. 2). Two half circles on either side of the Si beams represent the pins to apply the bending action. The pins are modeled to have a radius of 2 mm. The inner pins are separated by a distance of 32 mm while the outer pins are separated by 45 mm. The upper Si strip is made shorter to simulate a pre-crack situation. Isotropic elasticity is assumed for the Si with an elastic modulus of 169 GPa and Poisson's ratio of 0.28. This assumption is justified considering the stress state in the sample during bending and it enables us to compare the numerical results with the mathematical solution.

The Si strips are meshed using an 8-node 2D element PLANE183 (cf. Fig. 2). The pins utilized to apply the bending action are considered rigid. Line contact elements CONTA172 are furnished on the upper and lower surface of the Si strips where the pins come in contact with the sample, while a TARGE169 element is furnished on the lines representing the pins. Sliding contact is applied between the pins and the Si beams.

The same contact and target elements (CONTA172 and TARGE169) are furnished at the interface between the Si strips to ensure bonded contact. Furthermore, the cohesive zone model CZM is applied at this interface to model delamination during sample bending.

During the simulation, the lower pin is fixed while the upper pin is pushed downwards to bend the sample. The analysis is performed under plain strain assumption.

3.1. Cohesive zone model (CZM)

The CZM employed in this work has been developed by Alfano and Crisfield [19]. They assumed a bilinear law to relate traction to relative displacement of the delaminated surfaces. This approach can be linked to linear elastic fracture mechanics LEFM by acknowledging that the area under the triangle of the traction/relative displacement curve is equal to the critical energy release rate G_c. Further details are found in [19,20]. In the implementation of the model in FE, two quantities for every mode of fracture are required: The strain energy release rate G_c and the maximum traction τ, which is a threshold value after which damage (delamination) occurs. Special attention has to be paid to the choice of the value of τ. Choosing a very small value of τ will result in an artificial increase of the compliance of the system. On the other hand, choosing a too high value of τ will result in convergence difficulties and more refined mesh will be required in this case around the delamination front [19]. A rough estimate of such value can be obtained from the restoring load in the upper strip assuming it is a cantilever subjected to a constant bending moment and deflected by an amount proportional to the displacement of the moving pin (see Appendix A).

Interestingly, the value of τ has marginal effect on the shape of the extracted force curve, meaning that in all cases the calculated G_c from the curve value is independent of the input maximum traction τ (see Appendix A).

Delamination of samples in 4pb tests involves mixed mode of fracture [8]. Charalambides et al. [8] provided a detailed mathematical analysis of such a case and showed that a phase angle φ of about 41° is present in cases of equal strip thicknesses and same material properties. Accordingly, the input value of G_c to the FE can be properly divided to be utilized in the corresponding fracture modes.

3.2. Simulation and experiment for symmetric crack growth conditions

To validate the numerical results, a symmetric crack growth is simulated in plain strain case where the mathematical solution is provided in [8]. Symmetry boundary conditions are forced on the left side of the lower Si strip; see Fig. 2. The

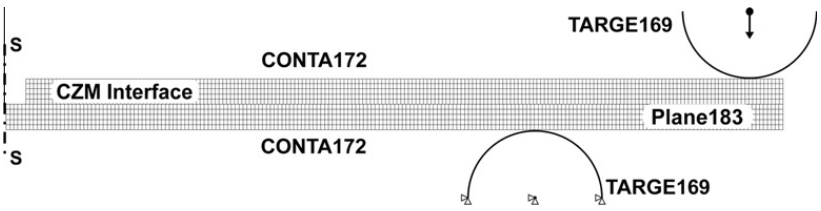

Fig. 2. Validation model of 4pb test. The locations of different elements and the boundary conditions utilized are shown. CZM is applied at the interface contact elements between the upper and lower beams.

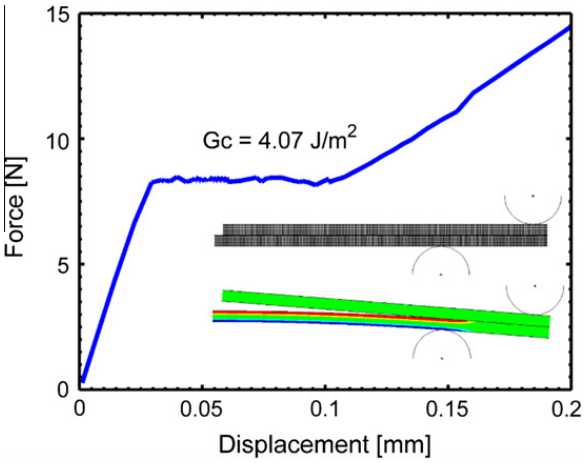

Fig. 3. Extracted force curve from the 4pb simulation. After elastic loading, the force reaches a plateau that can be utilized to calculate G_c using Eq. (1). The calculated G_c is in very good agreement with the value utilized in the simulation with an error of 1.75% ensuring the adequacy of the model. The inset shows the undeformed and x-component stress distribution of the deformed beams.

upper strip is made slightly shorter to simulate the presence of a pre-crack. A value of 4 J/m^2 for G_c is employed in the simulation.

Fig. 3 shows a typical force curve for an ideal 4pb test extracted from the simulation. The force curve shows three distinctive zones; initial elastic loading with a high stiffness because of the absence of delamination, followed by a force plateau where crack is propagating, and finally, further elastic loading with a much lower slope due to delamination.

Applying Eq. (1) to the plateau force value results in a G_c value of 4.07 J/m^2 (error of 1.75%) which is in very good agreement to the value employed in the simulation. This ensures that the CZM and mesh size adequately describes the 4pb problem. A literature benchmark study [1,21] shows that a typical precision level of a standard deviation of approximately 10% of the average G_c, is normally attained. Accordingly, given our accuracy level of the estimated G_c value and the overall force curve shape, we utilize this mesh size to address the rest of the problems.

It is worth mentioning that the force curves generated from the FEM are not smooth. This can be explained by the high nonlinearity of the problem characterized by snap-throughs and snap-backs [19] requiring sophisticated incremental algorithms and extreme fine meshes at the crack front.

The results of FE give a better insight in investigating the crack propagation in 4pb tests by monitoring the crack propagation length as a function of the pin displacement. Experimentally, a camera based gap length measurement system is employed here to estimate the crack growth rate. An image processing algorithm monitors the gap size between the upper and lower beams. The measured gap can be related to the crack length in the 4pb test as follows [18]:

$$a = \sqrt{4g^2 + \frac{Eh^3 b}{3PL_i} g}, \tag{2}$$

where g is the measured gap, P is the force, L_i is the inner pins separation. The location of the gap measurement has to be taken into account.

Monitoring this quantity experimentally can help in studying crack propagation dynamics by relating it to the speed of the moving pins. Fig. 4a compares Eq. (2) with the numerical results. In the FEA the gap size is recorded at an arbitrary location and Eq. (2) is employed to calculate the crack length. This value is compared to the extracted crack length from the FE by monitoring the position of the crack tip. Excellent agreement is observed in the curve ensuring the accuracy of Eq. (2).

Fig. 4b illustrates a crack length curve as a function of the pin displacement in a 4pb test extracted from FEM. It is seen that the curve starts at a value different from zero in our case due to the presence of a pre-crack. The crack remains roughly at a constant value until delamination starts where a linear increase in crack length is observed with a steep slope. When the crack approaches the position of the inner pin a significant reduction in the crack propagation slope is noted, however, the crack propagation rate remains linear.

The experimental crack length measurements are compared to the numerical results as seen in Fig. 4b. The plot shows a jump in the crack length to about 4 mm after which the previously mentioned behavior is observed. It is interesting to note that both cracks are propagating symmetrically even after reaching the inner pins location. The crack speed can be estimated by the slope of crack length plot to be 200 times the speed of the moving pin $\approx$50 μm/s.

With the previously mentioned observations, FEM can now be utilized to study more complicated situations found in real experiments that deviate from the assumptions regarding the symmetry of crack growth.

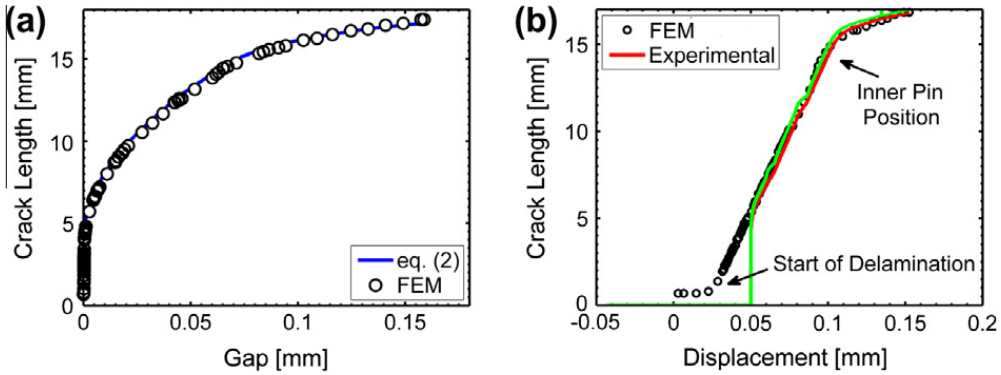

Fig. 4. Crack length determination: (a) verifying the accuracy of Eq. (2). The gap values are recoded from the FE simulation and crack length is calculated using Eq. (2). This is compared with the crack length extracted directly from the FE simulation by recording the position of the crack tip. Excellent agreement is observed indicating the accuracy of the equation (taking into account the location where the gap is measured). (b) Crack length plot shows the start of delamination in FEA. Crack grows linearly with the pin motion till the crack approaches the inner pin location where it slows down and propagates at a much slower rate. The experimental crack length measurement (Eq. (2)) for a symmetric crack growth agrees very well with the numerical results.

4. Results and discussion

4.1. Different pre-crack length

Statistical variation of the sample properties or misalignment in sample positioning might result in favoring of crack initiation on one side of the sample before the other. FE simulation can be employed to study the effect of this asymmetry on the extracted force curve and the estimated G_c.

A complete sample is simulated where two different pre-crack lengths are introduced. The short crack is 1 mm (right side) while the long one is made to be 4 mm (left side) as shown in the inset of Fig. 5. The pin is pushed downwards to 200 μm and the force curve is extracted. A value of 4 J/m^2 for G_c is used as an input into the simulation.

Fig. 5a shows the extracted force curve at every pin and the resultant load. The pin on the short pre-crack side recorded higher stiffness till the crack started to propagate, after which a drop in the load is observed. We can see that the two pins indicated the same load at a pin displacement of 60 μm. On the other hand, there is no clear effect of the asymmetry of pre-crack length on force curve. The G_c value obtained still equals 4.05 J/m^2 with very good agreement with the value employed in the simulation. This shows that the extracted results are insensitive to the asymmetry of the pre-crack length.

Monitoring the crack growth with the pin displacement explains the behavior of the force curves recorded at each of the bending pins. The short crack started to open earlier at a pin displacement of about 40 μm. The longer crack followed at a displacement of about 60 μm. The two cracks advanced together at the same rate till they approached the inner pin where they both changed the rate of crack growth as shown in Fig. 5b.

It is important to mention that, these results are obtained from static analysis of a delamination problem where equilibrium is achieved at every calculation substep. The asymmetry of crack growth can show different results if we include the dynamics of the problem into consideration. It is well known that the 4pb experiments must be performed as slow as possible to obtain an accurate estimation of G_c [5]. Consequently, our results should be generally applicable to real experiments.

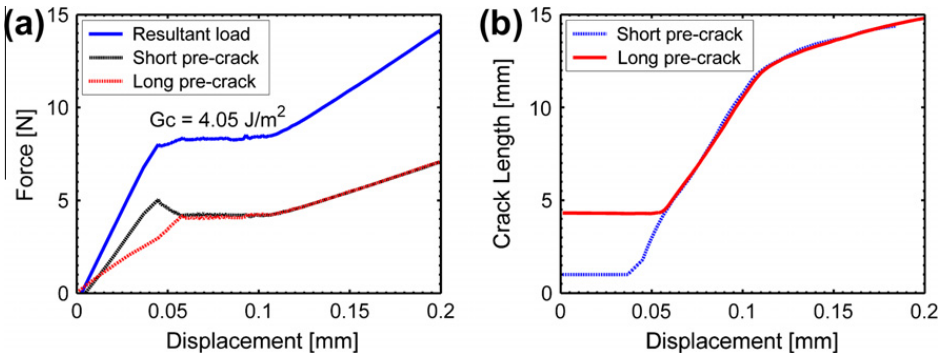

Fig. 5. (a) Extracted force curve from a 4pb simulation in a case of pre-crack asymmetric. The force curve is not affected by such non-ideality and the G_c value of the force plateau is in very good agreement to the value employed in the simulation (error of 1.25%). The recorded force on short pre-crack side indicates higher elastic stiffness followed by load reduction when the crack started propagating. (b) Crack propagation in asymmetric crack growth. The pre-cracks start delamination at different positions of the moving pins; however, they meet to propagate linearly approaching the inner pins after which they both continue propagating at an equal rate with a different slope.

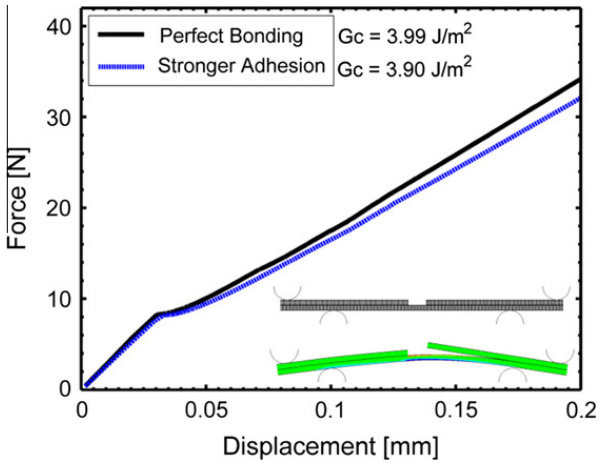

Fig. 6. Numerical force curves in case of single side crack propagation. In case of perfect bonding or a strong adhesion between the two beams, similar force curves are extracted with no clear force plateau. Taking the end point of the linear loading as the critical force to calculate G_c results in a proper estimation of G_c. The inset shows the single side delamination with the x-component stress distribution of the deformed beams.

A more extreme case is studied that is occasionally observed in real experiments which includes a crack opening on one side only. In our simulation, this is taken into account by two methods: full bonding of the Si strips on the closed side, or as a more realistic case by employing a high value of τ on the closed side. The G_c value of both sides is kept at 4 J/m^2. The pre-crack length is kept equal as well.

The force curve extracted from the simulation does not show a plateau as shown in Fig. 6. The initial elastic loading of the beam is linear followed by a sharp nonlinear change in the load rate that ends up with a linear increase again at a different slope. Calculating the G_c curve shows that using the end point of the initial elastic loading as a measure of G_c is a fairly accurate decision with an error of about 2.5%.

Studying the force recorded by the lower pin on the crack side reveals a very interesting finding. The sample loses contact with the pin and the test is transformed to a 3pb. This is confirmed by Fig. 7 where the load reaches a peak at about 30 μm then it gradually drops to zero. On the other hand, the reaction load recorded on the other pin shows a continuous increase on the recorded load. The inset in Fig. 7 confirms the loss of contact.

4.2. Crack propagation at different interfaces

It is possible in 4pb tests of multilayer structures that the crack jumps into the film stack at different interfaces on both sides. It is of interest to analyze such a case using the force curve.

The FE study of such test is conducted by applying two different G_c values on both sides. A G_c value of 4 J/m^2 is applied to one side while a 6 J/m^2 is applied to the other. The extracted force curve shows an extra feature where a force increase zone after the elastic loading of the sample is observed. The curve then shows a plateau at higher force, meaning that the soft interface opened first generating a single sided crack. The overall compliance of the system increased introducing a new slope to the force curve till the other side started to delaminate after which the force reached a stable value as seen in Fig. 8a.

The calculated G_c values indicate that the elastic loading ends at a G_c of 4.45 J/m^2 close to the low G_c utilized in the simulation. Subsequently, the force plateau stabilizes at a G_c of 5.7 J/m^2 also close to the high G_c employed in the simulation. Such observations indicate that the extracted G_c values of the force curves lie between the true G_c values of the two interfaces but with a significantly large error of about 10%. This is observed experimentally in the force curve shown in Fig. 8b. The curve shows a transition between two plateaus where the smaller value of the calculated G_c results in an overestimation of about 9% compared to the symmetric crack propagation in the same film stack. Note that the two force curves are different in the initial elastic loading. This is due to the fact that the numerical simulation assumes the presence of a pre-crack, while experimentally; the sample is notched to promote crack initiation that is accompanied by a load drop in force curve after the elastic loading.

The crack length plot reveals an interesting feature. The two cracks started from the same point; however the stronger interface (higher G_c) is delayed to start the crack propagation as seen in Fig. 9a. This results in a shift between the two curves. This can be utilized as an indicator to a crack propagating at different interfaces. These observations are clearly demonstrated in the experimental results in Fig. 9b where the linear regions overlap to the force plateaus in Fig. 8b. Interestingly, calculating the crack propagation speeds in this case results in 66.5 μm/s and 71.2 μm/s for the low G_c and high G_c sides, respectively. This is significantly larger than the symmetric value obtained before. These increased values of the crack speed can give rise to increased load values, and consequently to an overestimation of G_c, since dynamic contributions to G_c during crack propagation can become significant. Therefore it is critical for getting reliable G_c parameters in real experiments to keep the crack speed underneath critical levels.

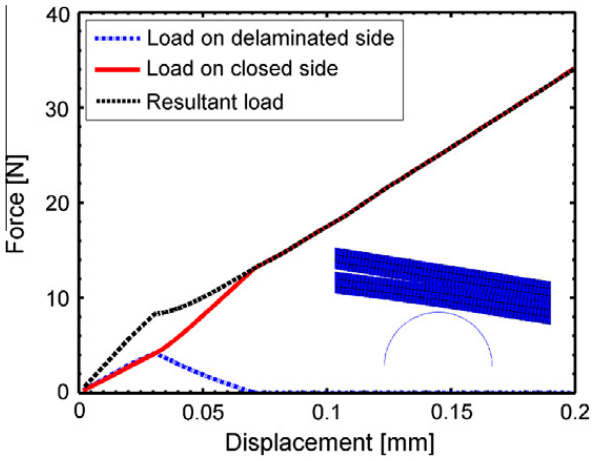

Fig. 7. Numerical force curves recorded at the lower pins and the resultant force curve in case of single side crack propagation. The force on the lower pin on the crack side reached zero at about 70 μm upper pin displacement, meaning that the test is transformed into a 3pb. The inset shows the physical loss of contact of the beam and the lower anvil.

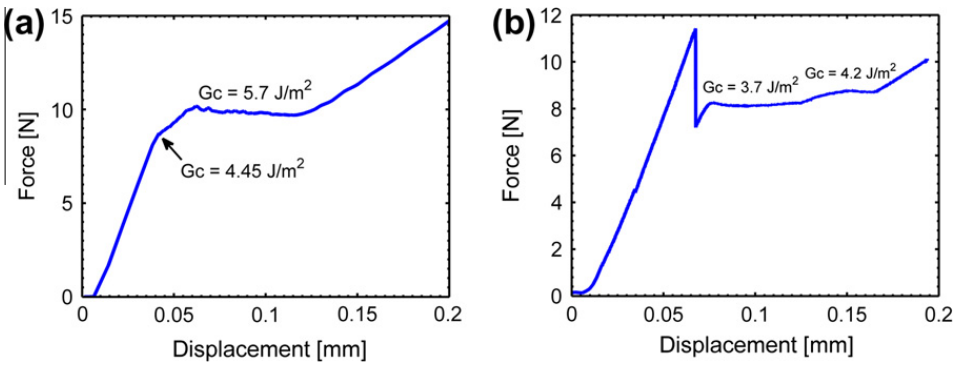

Fig. 8. (a) Numerical force curve for two cracks propagating at two different interfaces with G_c 4 and 6 J/m^2. The force plateau gives a erroneous value to the G_c with an error of about 10% of the maximum value. If the end of the elastic loading point is taken as the critical force an over estimation of G_c is observed. A corresponding measurement curve is shown in (b). Clearly visible are two partial plateau regions, corresponding to crack propagation in different interfaces. The low G_c value has an overestimation than the symmetric case by 9%.

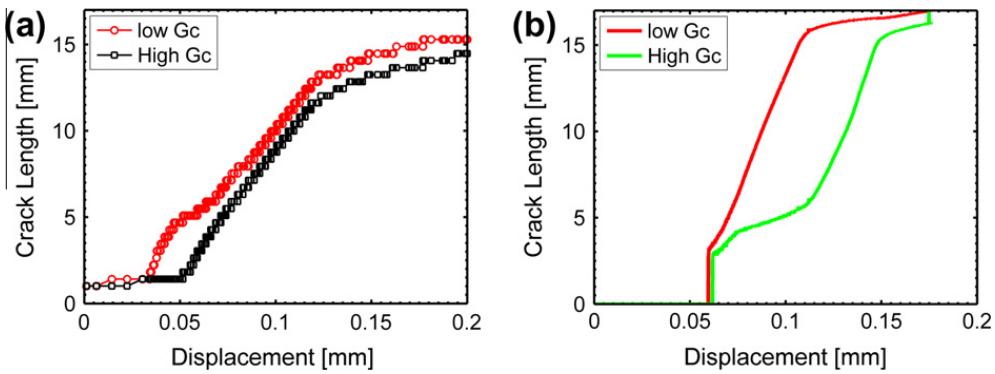

Fig. 9. (a) Numerical Crack length estimation in case of crack propagation in interfaces with different G_c of 4 and 6 J/m^2. The crack at the high G_c side is delayed to propagate resulting in a gap between the crack length curves on both sides. The cracks do not coincide at maximum pin displacement. This curve can be utilized as an alarm to such non-ideal situation. A measurement curve (corresponding to Fig. 8b) is shown as red and green line for the left and right crack, respectively (b). The regions of linear slope match with the regions of the partial plateaus in Fig. 8. Note that both cracks are propagating consecutively, each have a higher slope (speed) compared to the case of symmetric crack propagation in Fig. 4b. (For interpretation of the references to colour in this figure legend, the reader is referred to the web version of this article.)

5. Conclusion

The fundamental equation of estimating the critical energy release rate G_c in 4pb tests can be widely extended to situations that deviate from the basic idealized one. Using FEM, non-ideal situations were modeled including asymmetric pre-crack length and single sided crack propagation. The numerical force curve in case of asymmetric pre-crack did not show a clear deviation from the symmetric one; however, the force curve in the case of single sided crack propagation showed no force plateau. In both cases, the application of the fundamental equation resulted in an accurate estimation of G_c. When studying crack propagation at two different interfaces with different G_c values, the force curve showed a transition between two stable regions where the estimated values of G_c suffered of significant error.

Monitoring crack length as a function of pin displacement can be of a great value to explain different features in the force curve, to estimate crack speeds and to identify any deviations from the ideal test situation. This was demonstrated in the case of crack propagation at interfaces with different G_c values where a gap between the crack plots was observed and the plot indicated a large crack propagation speed.

Appendix A

As the aim of the study is to find the values of G_c for our tests, an independent estimation of the maximum traction τ has to take place. It is observed that choosing a very small value of τ will result in an artificial softening of the sample as shown in Fig. A1. This is evident in the elastic nonlinear initial loading of the force curve. On the other hand, choosing too high value of τ will result in convergence difficulties and more refined mesh is required around the delamination front [19]. Fig. A1 shows that force curves at high values of τ become identical and the initial loading portion becomes straight as it is supposed to be, but more convergence steps are needed in the numerical calculations especially when delamination starts.

It is noted that the value of τ has marginal effect on the plateau of the extracted force curve, meaning that in all cases the calculated G_c value is independent of the input maximum traction τ. A good estimate of such value can be obtained from the restoring force in a cantilever subjected to a constant bending moment and deflected by an amount proportional to the displacement of the moving pin. This is described in the next section.

Delamination of samples in 4pb tests involves mixed mode of fracture [8]. Charalambides et al. [8] provided a detailed mathematical analysis of such case and showed that a phase angle φ of about 41° is present in case of equal strip thicknesses and same material properties. Knowing that:

$$\varphi = \tan^{-1}\left(\sqrt{\frac{G_{II}}{G_I}}\right), \tag{A1}$$

and

$$G_c = G_I + G_{II}, \tag{A2}$$

a given value of G_c can be split into its two components using Eqs. (A1) and (A2) to be employed in the CZM model. Fig. A2 illustrates the effect of employing different G_c values in the numerical simulations. It is clear that with a higher G_c, higher force plateau is attained and the length of the plateau increases meaning that more sample bending is needed to force the crack to propagate.

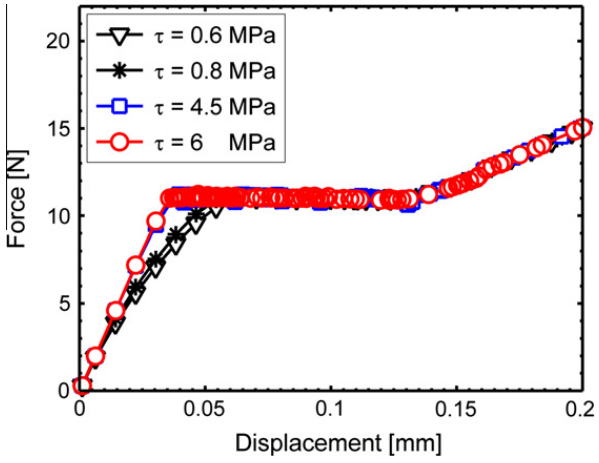

Fig. A1. Numerical force curves calculated with the same G_c value but at different maximum traction τ. Very small values of τ results in an artificial softening of the system. This is observed in the nonlinear initial elastic loading of the force curve. By increasing the value of τ the force curves become identical but with extra computation steps in FEA. In all cases the force plateau level is the same.

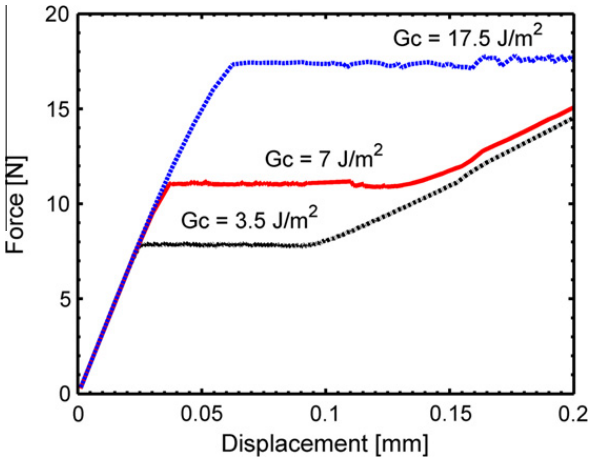

Fig. A2. Numerical force curves showing the effect of changing the G_c value of the force plateau.

Fig. A3. Schematic representing a cantilever deflection due to a bending moment. This can approximate the situation of the upper beam during the 4pb test.

A.1. Estimation of maximum traction τ

The value of the maximum traction employed in CZM is important to accurately describe the overall compliance of the test sample. This value can be estimated by calculating the force stored in the upper strip of the sample during bending.

If we assume that the upper strip of the sample resembles a cantilever under bending, the bending moment of the deflected cantilever can be expressed as follows:

$$M = \frac{2EI\delta}{l^2} \tag{A3}$$

where E is the elastic modulus of the strip, I is the moment of inertia, l is the cantilever length and δ is the cantilever deflection. The moment of inertia of the cantilever can be calculated as $I = bh^3/12$ where h is the cantilever height b is its depth. This is described in Fig. A3.

The cantilever length can be linked to the sample upper beam in 4pb considering the inner pin distance L_i and the a pre-crack length c to read:

$$l = \frac{L_i}{2} - c. \tag{A4}$$

In order to estimate the cantilever deflection δ, the deflection of beam under 4pb has to be known as a function of the pin displacement. Employing Euler–Bernoulli beam theory, the deflection curve for a simply supported beam under 4pb is as follows:

$$w(x) = \frac{3PLx}{Ebh^3}(L_i - x), \tag{A5}$$

and the slope of such curve can be evaluated at the inner pins from the following relation:

$$\left.\frac{dw}{dx}\right|_{x=0} = \frac{3PL}{Ebh^3}L_i \tag{A6}$$

Assuming that the portion of the beam between inner and outer pins remains straight during pin motion, we can relate the pin displacement to the bending force by multiplying Eq. (A6) by the pins separation:

$$y = \frac{3PL}{Ebh^3}L_i \times L, \tag{A7}$$

The beam deflection at the pre-crack tip ($x = L_i/2 - c$) can be estimated from Eq. (A5) to be:

$$w|_{x=\frac{L_i}{2}-c} = \frac{3PL}{Ebh^3}\left(\left(\frac{L_i}{2}\right)^2 - c^2\right). \tag{A8}$$

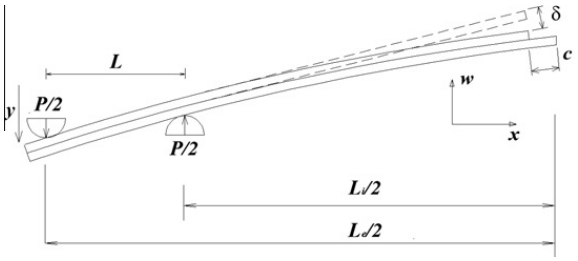

Fig. A4. A schematic showing different parameters of a double beam under 4pb.

Substituting the expression of P from Eq. (A7) into Eq. (A8), the deflection at the pre-crack tip can be related to the pin displacement:

$$w|_{x=\frac{Li}{2}-c} = \frac{y}{L-L_i}\left(\left(\frac{L_i}{2}\right)^2 - c^2\right). \tag{A9}$$

Now, we can derive the expression for the cantilever deflection δ from the difference between the position of the cantilever if it was not bent and the deflection of the beam as shown in Fig. A4. The deflection of the cantilever is:

$$\delta = \frac{l}{L}y - w|_{x=\frac{Li}{2}-c} = \frac{l}{L}y - \frac{y}{L-L_i}\left(\left(\frac{L_i}{2}\right)^2 - c^2\right), \tag{A10}$$

where y is the total pin displacement as was shown in Fig. A4.

Finally, the bending moment is translated to the traction τ by utilizing the following relation:

$$\tau = \frac{2M}{LA}. \tag{A11}$$

where A is the cross sectional area of the element.

References

[1] Shaviv R, Roham S, Woytowitz P. Optimizing the precision of the four-point bend test for the measurement of thin film adhesion. Microelectron Engng 2005;82(2):99–112.
[2] Lee CC et al. Adhesion investigation of low-k films system using 4-point bending test. Thin Solid Films 2009;517(17):4875–8.
[3] Lee CC et al. Interfacial fracture investigation of low-k packaging using J-integral methodology. IEEE Trans Adv Pack 2008;31(1):91–9.
[4] Van Hal B et al. Cohesive zone modeling for structural integrity analysis of IC interconnects. Microelectron Reliab 2007;47(8):1251–61.
[5] Hughey MP et al. Four-point bend adhesion measurements of copper and permalloy systems. Engng Fract Mech 2004;71(2):245–61.
[6] Lane M et al. Plasticity contributions to interface adhesion in thin-film interconnect structures. J Mater Res 2000;15(12):2758–69.
[7] Dauskardt RH et al. Adhesion and debonding of multi-layer thin film structures. Engng Fract Mech 1998;61(1):141–62.
[8] Charalambides P et al. A test specimen for determining the fracture resistance of bimaterial interfaces. J Appl Mech 1989;56:77.
[9] Wang B, Siegmund T. A modified 4-point bend delamination test. Microelectron Engng 2008;85(2):477–85.
[10] Lee CC, Yang YW. Fracture prediction of dissimilar thin film materials in Cu/low-k packaging. J Mater Sci. Mater Electron 2010;1–9.
[11] Chiu TC, Lin HC. On the homogenization of multilayered interconnect for interfacial fracture analysis. IEEE Trans Compon Pack Technol 2008;31(2):388–98.
[12] Corigliano A, Allix O. Some aspects of interlaminar degradation in composites. Comput Methods Appl Mech Engng 2000;185(2–4):203–24.
[13] Camanho PP, Dávila CG. Mixed-mode decohesion finite elements for the simulation of delamination in composite materials. NASA-technical paper; 2002. p. 211737.
[14] Scheider I, Brocks W. Simulation of cup-cone fracture using the cohesive model. Engng Fract Mech 2003;70(14):1943–61.
[15] Gullerud A. Three-dimensional modeling of ductile crack growth in thin sheet metals: computational aspects and validation. Engng Fract Mech 1999;63(4):347–74.
[16] Hillerborg A, Modeer M, Petersson PE. Analysis of crack formation and crack growth in concrete by means of fracture mechanics and finite elements. Cem Concr Res 1976;6(6):773–81.
[17] De Borst R. Numerical aspects of cohesive-zone models. Engng Fract Mech 2003;70(14):1743–57.
[18] Hecker M et al. Crack propagation and delamination analysis within the die by camera-assisted double cantilever beam technique. In: Interconnect technology conference and 2011 materials for advanced metallization (IITC/MAM), 2011 IEEE, International; 2011.
[19] Alfano G, Crisfield M. Finite element interface models for the delamination analysis of laminated composites: mechanical and computational issues. Int J Numer Method Engng 2001;50(7):1701–36.
[20] Kohnme P. ANSYS help documentation. ANSYS, Inc.; 2003. p. 8. [Theory release].
[21] Lane M et al. Adhesion and reliability of copper interconnects with Ta and TaN barrier layers. J Mater Res 2000;15(01):203–11.